



Published in final edited form as:

Nat Struct Mol Biol. 2009 August ; 16(8): 853–860. doi:10.1038/nsmb.1647.

Structural insights into host GTPase isoform selection by a family of bacterial GEF mimics

Zhiwei Huang^{1,4}, Sarah E Sutton^{2,4}, Adam J Wallenfang², Robert C Orchard², Xiaojing Wu¹, Yingcai Feng¹, Jijie Chai^{1,3}, and Neal M Alto²

¹National Institute of Biological Sciences, Zhong Guan Cun Life Science Park, Beijing, China

²Department of Microbiology, University of Texas Southwestern Medical Center, Dallas, Texas, USA

³Department of Biological Sciences and Biotechnology, Tsinghua University, Beijing, China

Abstract

The *Escherichia coli* type III effector Map belongs to a large family of bacterial virulence factors that activate host Rho GTPase signaling pathways through an unknown molecular mechanism. Here we report direct evidence that Map functions as a potent and selective guanine-nucleotide exchange factor (GEF) for Cdc42. The 2.3-Å structure of the Map–Cdc42 complex revealed that Map mimics the GEF strategy of the mammalian Dbl family but has a three-dimensional architecture that is nearly identical to the bacterial GEF *Salmonella* spp. SopE. A comparative analysis between human and bacterial GEFs revealed a previously uncharacterized pairing mechanism between Map and the variable $\beta 2$ –3 interswitch region of Cdc42. We propose a GTPase selection model that is experimentally validated by the preferential activation Rac1 and RhoA by the *Shigella* spp. effectors IpgB1 and IpgB2, respectively. These results significantly expand the repertoire of bacterial GEF mimics and unify a GEF selection mechanism for host GTPase substrates.

Rho GTPases activate numerous signal transduction pathways that regulate diverse cellular processes including actin dynamics, cell survival, cell-cycle progression and gene expression^{1–4}. Each signaling event requires that Rho proteins function as bimolecular switches, shuttling between a GTP-bound active state and a GDP-bound inactive state. Interconversion of these two distinct conformations of Rho GTPases is primarily mediated by two classes of regulatory proteins: GEFs, which catalyze the exchange of GDP for GTP to activate Rho proteins, and GTPase activating proteins (GAPs), which accelerate the slow intrinsic GTPases' activity to inactivate them.

Reprints and permissions information is available online at <http://npg.nature.com/reprintsandpermissions/>

Correspondence can be addressed to N.A. (neal.alto@utsouthwestern.edu) or J.C. (chaijijie@nibs.ac.cn).

⁴These authors contributed equally to this work.

Accession codes. Protein Data Bank: Coordinates for the Map–Cdc42 have been deposited with accession code 3GCG.

Supplementary information is available on the Nature Structural & Molecular Biology website.

AUTHOR CONTRIBUTIONS

N.M.A., J.C., Z.H. and S.E.S. designed the research; Z.H., S.E.S., N.M.A. and J.C. performed the research; A.J.W., R.C.O., Z.W. and Y.F. provided new reagents and analytical tools and performed experiments; N.M.A. and J.C. wrote the paper.

The first mammalian GEF⁵ was nominated as Dbl because it was isolated from diffuse B cell lymphoma cells⁶. Several Dbl homology (DH) domain-containing proteins were subsequently shown to possess GEF activity with specificity for distinct Rho family GTPases including RhoA, Rac1 or Cdc42. Biochemical and structural studies have formulated some general schemes for GTPase isoform selection by Dbl family members. The nonconserved residues from the seat-back region of the DH domain were found to have a crucial role in defining the selectivity of GEFs through interaction with the variable residues, dubbed the ‘specificity patch’, from the three strands, β 1, β 2 and β 3, of Rho GTPases^{7,8}. For example, intersectin-1on (ITSN-L), a Cdc42-specific GEF, can be engineered to activate RhoA by substitutions of two residues from the seat-back region of the ITSN-L domain⁸. These support a ‘lock-and-key’ pairing mechanism between Dbl GEFs and their cognate Rho GTPases.

In several reported cases, bacterial pathogens have been shown to hijack host GTPase communication networks by delivering GEFs directly into host cells. For example, *Legionella pneumophila* subverts Arf GTPase signaling by ‘type IV’ delivery of RalF, a structural mimic of the human Sec7 GEF domain^{9,10}. In this case, it is clear that the pathogen has captured an ancient eukaryotic gene and thus shows the same signaling characteristics of mammalian Sec7. In contrast, the ‘type III’ secreted effector SopE of *Salmonella* spp. is a functional mimic of Dbl family Rho GEFs¹¹ but has no structural homology to any Dbl proteins¹². The ~160 residues of the SopE catalytic domain is composed primarily of α -helices that form a V-shaped structure. Key features of this GEF include a ‘catalytic loop’ that bisects the switch 1 and 2 loops of Cdc42 GTPase and a long helix that runs perpendicular to the catalytic loop and contacts the outer edge of both GTPase switch regions. Despite its structural deviation from Dbl, SopE potently activates Cdc42 by a conserved GEF mechanism¹².

Recently, a large family of bacterial type III effectors was found to regulate actin cytoskeletal dynamics through an unknown GTPase signaling mechanism¹³. The prototypic family member *E. coli* Map induced cell surface filopodia¹⁴, an actin-based phenotype regulated by Cdc42. Other family members, including *Shigella* IpgB1 and IpgB2 and *Salmonella* SifA and SifB, can discriminate between cellular phenotypes by selectively regulating RhoA, Rac1 or Cdc42 signaling pathways^{13,15,16}. On the basis of this remarkable functional diversity, Map and its family members were originally proposed to directly mimic Rho family GTPases^{13,17}. However, this mechanistic view was recently challenged by our group, with the reported crystal structure of *Salmonella* SifA¹⁶. Unexpectedly, about 150 residues from the C-terminal side of SifA form a close structural homolog of SopE, an observation that suggests their common activity as GEFs. SifA and SopE are genetically unrelated, and there has been no GEF activity demonstrated for SifA or any of the Map-related type III effectors. We set out to define the structural and functional relationship between the Map family type III effectors and the Rho family GTPases.

Here we report the GEF activity and the crystal structure of *E. coli* Map in complex with Cdc42. This structure captures the stable intermediate of a bacterial GEF–GTPase complex that can be directly compared to host GEF mechanisms, as well as the genetically unrelated GEF SopE. Further studies into the selection mechanism define the underlying principles of

host GTPase selection by several Map family members, including *Shigella* IpgB1 and IpgB2. These results significantly expand the repertoire of bacterial GEF mimics, reveal the underlying principles governing host GTPase substrate selection and provide compelling new insight into the evolution of pathogenic diversity at the molecular level.

RESULTS

Structural and functional analysis of Map as a Cdc42 GEF

As a prelude to this study, we screened several members of the Map/IpgB/Sif family for direct binding interactions with Rho family GTPases *in vitro* (data not shown). Notably, recombinant Map formed a highly stable protein complex with the nucleotide-free form of Cdc42 (Fig. 1a) but not with GST proteins. The nucleotide-independent binding profile of Map–Cdc42 interaction is consistent with GEF protein interactions with GTPase substrates. Map may therefore function as a GEF *in vitro*, a postulate that is supported by Map-induced host cellular membrane extensions known as filopodia, an actin-based phenotype that is regulated by Cdc42. Indeed, kinetic analysis of Cdc42 guanine-nucleotide exchange confirmed this notion. Map induced the release of GDP and facilitated new incorporation of GTP γ S by 31 ± 6 -fold over intrinsic guanine-nucleotide exchange on Cdc42 (Fig. 1b and Supplementary Table 1). These rapid GDP-GTP exchange kinetics are similar to those previously reported for the Cdc42-specific GEFs SopE¹¹ and human DBL⁵ (also known as MCF2) under similar experimental conditions (Supplementary Table 1). Previous studies from our laboratory have also indicated that the induction of actin filopodia by Map requires two residues found in the invariant WxxxE motif¹³. Mutations in Map-Trp74 and Map-Glu78 abolished Map binding to Cdc42 (Fig. 1a) and inhibited the exchange of GDP for GTP on Cdc42 (Fig. 1b).

Next, we solved the crystal structure of Map in complex with Cdc42 at 2.3-Å resolution (Table 1). Map is composed of seven α -helices that are arranged into one three-helix bundle (α 2, α 3 and α 7) and one four-helix bundle (α 1, α 4, α 5 and α 6), forming a V-shaped structure (Fig. 1c). Connecting the helix bundles is a long loop between α 3 and α 4 that we refer to as the ‘catalytic loop’ (residues 123–128) herein, on the basis of previous nomenclature¹². The two residues Map-Trp74 and Map-Glu78 of the previously defined WxxxE motif¹³ are located at the interface of the helix bundles (Fig. 1c) and contribute many interactions between them (not shown). These highly conserved residues probably function as crucial protein folding determinants upon type III delivery into host cells.

The interaction between Cdc42 and Map resulted in a 1:1 stoichiometric complex in the crystal structure and buried 2,727 Å² exposed surface area (Fig. 1c). Most of the residues in Cdc42 are well defined by the electron density, except for residues 27–30, which are presumed to be disordered in solution. Cdc42 is seated in the region around the juncture of helix bundles of Map with an extensive, although not complete, charge and surface complementarities (Fig. 1c).

Map recognition of Cdc42 switch 1 and switch 2

The crystal structure revealed that the major interaction surface of Cdc42 occurs around switch 1 and switch 2 (Fig. 1d and Supplementary Fig. 1). A large network of hydrogen bonds dominates the interactions at one side of the switch 1 contact interface (Fig. 1d). Four out of seven hydrogen bonds are formed between Map-Asp92 and the backbone amides of Cdc42-Thr35 and Cdc42-Val36, as well as the side chain hydroxyl group of Cdc42-Tyr32 (Fig. 1d). To strengthen the lining of switch 1 in Map, one pair of salt bridges is made between Cdc42-Asp38 and Map-Arg89. Two residues, Map-Ala127 and Map-Q128, found within the catalytic loop, further fortify the interaction of Map with switch 1 by making hydrophobic contact with Cdc42-Val36 and by forming a hydrogen bond with the backbone amide of Cdc42-Phe37, respectively. Although Map-His133 does not make interaction with Cdc42, it forms a strong intramolecular hydrogen bond with Map-Ala127 (with distance 2.8 Å), which may be important for maintaining the local conformation of the catalytic loop.

Packing of the C-terminal helical portion of Cdc42 switch 2 against the helices $\alpha 1$, $\alpha 2$ and $\alpha 4$ of Map seems to dominate the switch 2 interactions (Fig. 1d). This is primarily mediated by hydrophobic contacts of Cdc42-Leu67 and Cdc42-Leu70. In addition, several hydrogen bonds flank Cdc42-Leu67 and Cdc42-Leu70, which are centered in the interface. Notable contacts include those of Map-Gln77 of the WxxxE motif, which forms two hydrogen bonds with the main chain amides of Cdc42-Asp65 and Cdc42-Arg66 (Fig. 1d). Additional hydrogen bonds of the Map and Cdc42 switch 2 interface are outlined in Supplementary Figure 1.

Map regulates actin dynamics via intrinsic GEF activity

In full support of our structural observations, deletion of a conserved catalytic loop region 127–131 (Map AQSSI) or single mutations at Ala127 and Gln128 from the catalytic loop inhibited Map GEF activity *in vitro* (Fig. 2a) and abolished binding to nucleotide-free Cdc42 (Fig. 2b). In addition, mutations of numerous interface residues at Map helix $\alpha 2$ and the catalytic loop further confirmed their essential role in GEF activity of Map and its interaction with Cdc42 (Fig. 2a,b).

Previous studies¹³ have demonstrated that transient transfection of Map induced robust actin filopodia at the plasma membrane of 293A cells (Fig. 2c). By contrast, several interface mutations, including the catalytic loop deletion mutant Map AQSSI, the point mutant MapQ128Y and the $\alpha 2$ helix mutant MapD92A, compromised the host signaling function of Map (Fig. 2c). As a more physiological test of Map GEF function *in vivo*, we examined HeLa cell actin architecture surrounding enteropathogenic *E. coli* (EPEC) microcolonies 20 min after infection (Fig. 2d). We assessed Map's GEF activity by complementing *map* strains of EPEC with plasmid-expressed wild-type Map or the catalytically dead mutant MapQ128Y. Type III delivery of wild-type Map in complemented EPEC *map* strains produced transient filopodia in $60 \pm 4\%$ of HeLa cells; in contrast, this phenotype was nearly undetectable in the Map Q128Y mutant (Fig. 2d). Quantification of both transient transfection experiments and EPEC infection experiments are shown (Fig. 2e). Control experiments also confirmed that complemented mutant EPEC strains attached, colonized and formed actin pedestals similarly to wild-type EPEC (data not shown). Taken together,

these findings support the hypothesis that Map functions as a Cdc42 GEF during a natural *E. coli* infection.

Comparison between bacterial and human GEFs

We found *Salmonella* SifA to be the closest structural homolog to Map, with an r.m.s. deviation of 3.0 Å over 132 Ca atoms. In addition, *Salmonella* SopE is also structurally related to Map, with an r.m.s. deviation of 4.2 Å over Ca 130 atoms. All three effectors share a V-shaped structure with a long catalytic loop that spans the two-helix bundles (Supplementary Fig. 2). As the structure of SopE has also been solved in complex with Cdc42 (ref. 12), we undertook a detailed comparison between Map, SopE and the human Dbl GEF intersectin 1 (ITSN)⁸ in complex with Cdc42.

Map and SopE share a similar overall architecture in complex with Cdc42 (Fig. 3a,b), whereas ITSN uses a completely distinct interaction surface (Fig. 3c). Notably, however, all three GEFs interact with switch 1 and switch 2 of Cdc42 in two common and fundamental ways. First, three negatively charged residues, Map-Asp92, SopE-Asp124 and ITSN-Glu1244, occupy a similar position on the surface of Cdc42 and form an identical set of interactions with switch 1 (Tyr32, Thr35 and Val36) as ITSN does (Fig. 3d). Similar interactions were also observed in other GEF-GTPase complexes^{18–20}, supporting the notion that these interactions involving switch 1 are highly conserved in all Rho GEF proteins. Second, the separate structures of all three GEFs with Cdc42 featured the hydrogen bonds formed between Map-Gln77 (SopE-Gln109 and ITSN-Asn1421) and the backbone amides of Cdc42-Asp65 and Cdc42-Arg66 (Fig. 3d).

Map, SopE and ITSN induce similar structural alterations in Cdc42 despite their lack of overall structural and sequence homology (Fig. 3e). Notably, each of these GEFs cause Cdc42-Ala59 from switch 2 to flip over toward the GDP-binding region, thus occluding the Mg²⁺-binding site and blocking the productive Mg²⁺ binding and concomitant release of GDP (Fig. 3f). As in other GEF-GTPase structures, such a conformation around Cdc42-Ala59 is stabilized via a pair of salt bridges formed between Cdc42-Glu62, which flips almost 180° following Map binding, and Cdc42-Lys16 (Fig. 3f). The conformational changes around Cdc42-Ala59 and Cdc42-Glu62 are believed to have an important role in facilitating the release of GDP³, indicating that there are conserved nucleotide-exchange mechanisms between Map, its family members and other GEF proteins.

The β2–3 interswitch as a potential site for GEF selection

Whereas Map induces host cell actin filopodia through Cdc42 activation, SopE promotes *Salmonella* invasion in a Rac1- and Cdc42-dependent manner. It is currently unknown how such GTPase isoform specificity is achieved by bacterial GEF mimics. Structural comparison showed that Map and ITSN induce similar conformational changes around switch 1 and β2–3 of Cdc42 (Fig. 4a). In contrast, SopE induced a substantially different conformation around these regions, with a notable difference in the position of Cdc42-Tyr40 (Fig. 4a). Whereas SopE directly engaged Cdc42-Tyr40, neither Map nor any other known Rho GEF provided similar interactions with Cdc42. Instead, Tyr40 is rotated around its Ca atom by ~90° away from the Map-Cdc42 interface, similarly to the position of that residue

in human GEF-Rho GTPase structures (Fig. 4a). It is important to note that SopE residues Ile177 and Gln194, which engage Cdc42-Tyr40, are appositional to Map residues that contact Cdc42 β 2–3 (Fig. 4b,c). For example, Map-Gln136 from the α 4 helix made hydrophobic contacts with Cdc42-Phe56 of the β 3 strand (Fig. 4b). Moreover, Ile156 and Phe159 from the α 6 helix of Map engaged in extensive van der Waals contacts with four β 2–3 residues of Cdc42 (Ala41, Thr43, Thr52 and Phe56) (Fig. 4b). This extensive hydrophobic interface resulted in a 4.8-Å displacement of the Ca atom of Cdc42-Gly47 (found at the tip of the β 2–3 hairpin) toward the solvent-exposed area, compared to the Ca atom of the GDP-bound Cdc42 (Fig. 4a). Analogous conformational changes in GTPases are induced by the human GEFs (ITSN and DBL) and Map (Fig. 4a)^{8,20,21}, suggesting the possibility that β 2–3 has a conserved role in GTPase recognition by both eukaryotic and bacterial GEF mimics.

It has been reported that Dbl GEFs distinguish between GTPase isoforms by complementary pairing with their unique β 2–3 hairpin sequences^{7,8,20}. Thus, the α 4 and α 6 regions of Map that interact with the β 2–3 hairpin of Cdc42 may be readily used as the discriminatory element for Cdc42. To test this idea, we superimposed the structures of Rac1 and RhoA onto the Map structure around the β 2–3 region of Cdc42 (Fig. 4d). On the basis of these models, the α 4 helix residue Map-Gln136 is predicted to engender steric clashes with the bulkier side chain Rac1-Trp56 or RhoA-Trp58 of the equivalent β 3 residue, Cdc42-Phe56. In addition, substitutions of β 2–3 Cdc42-Thr43 and Cdc42-Thr52 with their corresponding larger residues of Rac1 (Asn43 and Asn52) or RhoA (Asp45 and Glu54) would collide with Map-Pro155, Map-Ile156, Map-Arg158 or Map-Phe159 found at the N-terminal portion of helix α 6 (Fig. 4d). Because the switch loops are nearly identical among GTPase isoforms, whereas the β 2–3 residues are variable (Supplementary Fig. 3), the structure-based model predicted that Map activates Cdc42 in a highly selective manner.

Map recognizes Cdc42 through a lock-and-key pairing mechanism

To experimentally test the structural models, we incubated nucleotide-free RhoA, Rac1 and Cdc42 (all GST tagged) with recombinant Map and isolated the resulting protein complexes by glutathione agarose pull-down. Map bound exclusively to Cdc42 but not RhoA or Rac1 (Fig. 5a), as predicted by the modeled structure. Map also had GEF activity for Cdc42, but not for RhoA or Rac1, further confirming this notion (Fig. 5b,c). To determine whether the variable β 2–3 residues defined the isoform selection by Map, we directly substituted residues from β 2–3 Cdc42 for those in Rac1 or RhoA (Fig. 5b,c). Unexpectedly, no single substitution of a Cdc42 β 2–3 interface residue to that of RhoA or Rac1 was sufficient to inhibit its interaction with Map (data not shown). Therefore, we tested a combinatorial switch of Cdc42 β 2–3 residues to those found in Rac1 (A41S T43N T52N F56W) or RhoA (T43D T52E F56W) for Cdc42 activation (Supplementary Table 1). Compared to wild-type Cdc42, Map had a reduced activity against the mutant Cdc42 whose β 2–3 residues were switched to those of Rac1 (Fig. 5c), and no activity toward the mutant whose β 2–3 residues were switched to those of RhoA (Fig. 5c).

A comprehensive interaction set of Cdc42 β 2–3 isoform switch mutants (Fig. 5d) clearly demonstrated that the combination of Cdc42-Trp56 plus the smaller-sized residues in the

β 2–3 specificity patch accommodates Map by a lock-and-key complementary pairing mechanism. To positively validate such a mechanism, we introduced Cdc42 β 2–3 residues into the Rac1 (a GTPase that normally does not interact with Map) mutant S41A N43T N52T W56F and tested it for Map binding. These four substitutions converted Rac1 GTPase into a Map-binding protein (Fig. 5e) and allowed it to be modestly stimulated (4.9 ± 0.8 -fold) above wild-type Rac1 nucleotide-exchange rates (Supplementary Table 1). These structural and functional data validate a wealth of cellular studies demonstrating that Map selectively induces actin filopodia during EPEC infection^{13,14,22}, a phenotype directly regulated by Cdc42.

A diversity-generating ‘selection epitope’ in bacterial GEFs

The identification of a universal mechanism for GTPase isoform selection could have far-reaching consequences for our understanding of numerous bacterial pathogenic life cycles, including those of *E. coli*, *Salmonella* and *Shigella*. To explore this idea, we aligned 24 genes¹³, representing six general classes of bacterial type III effectors related to Map, based on primary sequence homology and conserved secondary-structural elements (Fig. 6a) around the regions of Map that interact with Cdc42. Whereas the surface-exposed Cdc42 switch 1 and 2 binding residues of Map are highly conserved between the family members (Fig. 6a,b, red residues), the α 4– α 6 residues that interact with the β 2–3 interswitch regions of GTPases were variable (Fig. 6a,b blue residues), suggesting that α 4– α 6 may function as a GTPase-discriminating element for the entire Map family. Experimental validation of this proposal was demonstrated from biochemical studies on *Shigella* IpgB1. Recombinant IpgB1 (residues 46–208) greatly accelerated the GTP exchange rate on Rac1 (32.5 ± 4 -fold) and had low but detectable exchange activity on Cdc42 (6.5 ± 2 -fold), whereas it had no activity on RhoA (Fig. 6c). The GTPase selection profile of IpgB1 was confirmed by glutathione pull-down experiments in which IpgB1 bound to Rac1 and Cdc42 but not RhoA (data not shown).

Next, we tested whether IpgB1 used a similar Rac1 selection mechanism as that described for Map-Cdc42. We engineered Cdc42 constructs in which the Cdc42 β 2–3 residues were replaced by the equivalent residues found in Rac1 (A41S T43N T52N F56W). IpgB1 stimulated GTP exchange for Cdc42 to the Rac1 β 2–3 mutant \sim 4.5 times faster than for wild-type Cdc42 (Fig. 6c and Supplementary Table 1). Additional combinatorial switch-of-function mutations are in full agreement with these data (Supplementary Fig. 4). Thus, IpgB1 differentially selects GTPases via complementary pairing to at least four β 2–3 strand residues that are specifically found in Rac GTPase isoforms.

The structurally and experimentally based model in which the α 4– α 6 helices govern GTPase selection correctly predicted that neither Map nor IpgB1 could bind or activate RhoA (Figs. 5 and 6c). Selection against RhoA probably resulted from three charged and bulkier residues—RhoA-Arg3, Rho-Asp45 and Rho-Glu54—generating a striking steric clash with the N-terminal side of the α 6 helix (Fig. 4d). Notably, the sequences of the α 4– α 6 specificity epitope in Map and IpgB1 have no positively charged residues (Fig. 6a), which are the major determinants for selection of RhoA by Db1 family GEFs⁸. We noticed that Map-Ile156 and Map-Phe159 are substituted for two basic residues (IpgB2-Arg142 and

IpgB2-Lys145) in *Shigella* IpgB2 and its closely related homolog EspM1 (Fig. 6a). Consistent with the model, IpgB2 showed marked activation of RhoA (22.2 ± 5 -fold) compared to the GTPase isoforms Cdc42 (4.5 ± 0.5 -fold) and Rac1 (6.5 ± 1 -fold) (Fig. 6d). In addition, recombinant expressed and purified IpgB2 (residues 20–188) bound directly to nucleotide-free RhoA and with weaker affinity to Rac1 and Cdc42 (data not shown). In further agreement with our selection mechanism, all of the type III effectors that activate RhoA signaling pathways in cells, including EspM2 and EspM3, have equivalent basic residues at the $\alpha 4$ – $\alpha 6$ selectivity epitope²³. Thus, a conserved type III effector GEF structure at $\alpha 4$ – $\alpha 6$ probably imparts pathogenic signaling diversity through complementary pairing to the $\beta 2$ – $\beta 3$ interswitch strand of distinct GTPase substrates (Fig. 6e).

DISCUSSION

Here we present compelling new evidence that the members of a large bacterial type III effector family function as GEFs for Rho GTPases. The crystal structure of Map in complex with Cdc42 revealed that these effectors mimic the function of human Dbl GEFs through structural architecture similar to that of *Salmonella* SopE. We also found that *E. coli* Map and *Shigella* IpgB1 and IpgB2 generate remarkable GEF diversity through differential recognition of the $\beta 2$ – $\beta 3$ specificity patch of Cdc42, Rac1 and RhoA, respectively. This lock-and-key pairing mechanism seems to mimic the selection strategy of human Dbl family GEFs^{7,8}, clearly demonstrating the sophistication of bacterial GEF proteins (Fig. 6e).

Recent studies demonstrate that *Shigella* IpgB1 participates in the invasion of nonphagocytic epithelium through the selective activation of Rac1 (refs. 15,24). In contrast, the attaching and effacing pathogen group, including EPEC and EHEC O157:H7, type III secrete Map proteins that specifically activate Cdc42. Because Rac1, and not Cdc42, facilitates phagocytic cup biogenesis through actin lamellipodia signaling, it is possible that the interconversion between extracellular and intracellular pathogenesis relies on the simple switch of GTPase diversity by Map and IpgB1, respectively. In support of this diversity-generating mechanism, the type III effectors SifA and SifB have integral roles in membrane trafficking and positioning of the replication vacuole of *Salmonella*^{25–28}. These bacterial effectors probably discriminate between GTPase substrates, possibly beyond the Rho family, to promote an intracellular pathogenic life cycle. It is therefore intriguing to suggest that Map and its family members have simultaneously maintained a universal guanine nucleotide-exchange mechanism for GTPase activation and evolved a pliable GTPase isoform selection mechanism for the exploitation of new host cell niches.

The type III effector *E. coli* Map was reported to function as an activated Cdc42-like protein to induce actin-based signaling in host cells¹³. Clearly, the data presented here support the role of Map as a GEF rather than a GTPase itself. However, it is likely that Map is found in discreet microdomains or signaling complexes that couple GTPase activation to specific GTPase effector signaling pathways. Indeed, several lines of evidence support a highly sophisticated mechanism for Map signaling^{13,22,29}. In addition to its SopE-like GEF domain, Map harbors a PDZ (PSD-95/Dlg/ZO-1)-interaction motif at its C terminus. This motif binds directly to the PDZ protein Ebp50, an apically localized scaffold that couples ion channels and transporters to the actin cytoskeleton. A deletion of the C-terminal PDZ

interaction motif, or small interfering RNA knockdown of Ebp50, inhibits actin polymerization induced by Map^{13,22}. Approximately 37% of human GEF proteins (26 of 70) have PDZ ligands at their C terminus³⁰, suggesting that bacteria have co-opted a common GEF signaling mechanism. It is likely that the PDZ scaffolds couple GTPases directly to downstream targets as a mechanism of ensuring signaling specificity and fidelity. Future studies will be needed to address how these mechanisms coevolved between bacteria and host, and to what extent scaffolding interactions participate in conferring pathogenic diversity. Nevertheless, our findings demonstrate that the bacterial GEF protein structure is a common, tractable and genetically inherited module that is exploited by numerous enteric bacteria to generate GTPase signaling diversity in host cells.

ONLINE METHODS

Plasmids

We carried out in-frame PCR cloning of the *map* gene from EHEC O157:H7 (accession no. AP002566), IpgB1 (accession no. NC_002698) and IpgB2 (accession no. NP_085292) from *Shigella flexneri* into a modified His₆-myelinating basic protein (MBP) fusion vector with a pet28B backbone or pGEX-6p. Bacterial expression clones encoded residues 37–203 of Map, 46–208 of IpgB1 and 20–188 of IpgB2. We cloned Rho GTPases into pGEX-6p, pGEF-4T1 or pCool, a modified pGEX 4T vector with a tobacco etch virus (TEV) cleavage site. Detailed plasmid information is available upon request. For mammalian expression, full-length *map* was subcloned into pEGFP-C2 (Clontech) using PCR. All mutants were generated using the QuickChange Site-Directed Mutagenesis (Stratagene) kit, following manufacturers' instructions, and confirmed by sequencing.

Protein expression and purification

His₆-MBP-tagged Map, IpgB1 and IpgB2 were expressed in *E. coli* BL21 (DE3) cells using 0.4 mM IPTG for 18 h at 16 °C. Cells were pelleted, resuspended in TBS/DTT buffer (TBS with 1 mM DTT and complete EDTA-free protease inhibitor tablets (Roche)), emulsified on ice three times, and clarified by centrifugation at 30,000*g* for 30 min at 4 °C. His₆-MBP-tagged proteins were purified on Ni-NTA beads following the manufacturers instructions (Qiagen). Protein samples (0.5 ml of a 10 mg ml⁻¹ solution) were injected into a 24-ml bed volume Sephadex-200 column interfaced to an AKTA FPLC (Amersham), and 0.5-ml elution fractions were collected. Fractions containing monomeric type III effectors were detected by spectrophotometric analysis (at 280 nm) and SDS-PAGE, collected and concentrated to 1 mg ml⁻¹. Samples were snap frozen and stored at -80 °C in a final concentration of 10% (v/v) glycerol. GST-tagged Rho GTPases were purified on glutathione-Sepharose beads as described³¹. Mutant Cdc42 proteins were purified by anion-exchange column (Source-15Q, Pharmacia) and gel filtration chromatography (Superdex200, Pharmacia) after removal of GST by Precision protease (GE Healthcare Life Sciences).

GST pull-down and guanine nucleotide-exchange assays

For GST pull-down assays, Glutathione Sepharose beads (25 µl) were incubated with 10–200 µg GST-tagged RhoA, Rac1 or Cdc42 and stripped of nucleotide by incubating the

beads with TBS/DTT and 10 mM EDTA. GTPases were washed in TBS containing 1 mM EDTA and 1% (v/v) Triton-X 100. Bacterial type III effector proteins (10 μ g) were incubated with the GTPases for 1 h at 4° and washed three times with TBS/DTT Triton buffer. Protein interactions were analyzed by SDS-PAGE and Coomassie staining. Guanine nucleotide-exchange assays were conducted as reported³² using concentrations between 100 nM and 1 μ M bacterial effectors and 1 μ M GTPases. Fold induction is presented as the rate of initial velocities (slope from 0 time to 30 s) for the experimental condition over the initial velocity of intrinsic GDP-GTP exchange on native GTPases. The s.e.m. from at least three independent experiments is presented.

EPEC infection and indirect immunofluorescence

Wild-type EPEC E2348/69 and EPEC *map* strains were obtained from B. Kenny³³. Complementation plasmid pBBR1MCS1 carrying the *map*, *map AQSSI* or *mapQ128Y* gene was introduced into EPEC *map* strain (B. Kenny) by electroporation. HeLa cells were infected with EPEC strains for 20 min with pre-activated EPEC, as described¹⁴. GFP-Map and mutant transfected cells were processed and stained as described³⁴. Briefly, cells were fixed and then stained with Rhodamine-phalloidin to detect cellular actin. Microscopy was performed on a Zeiss Axiovert microscope (Carl Zeiss Microimaging) using a MicroMax digital camera (Roper-Princeton Instruments) controlled by MetaFluor software (Universal Imaging). Optical filters were obtained from Chroma Technologies and 40 \times or 63 \times objectives were used for image acquisition.

Cdc42–Map complex formation for crystallization

All the constructs were generated by the standard PCR-based cloning strategy, and we confirmed their identities by sequencing. Map (residues 37–203) and human Cdc42 (residues 1–181), wild type or various mutants, were cloned into the vector pGEX-2T. All the proteins were expressed in *E. coli* strain BL21 (DE3). Cells were collected, pelleted and then resuspended in buffer A (25 mM Tris, pH 8.0, 150 mM NaCl, supplemented with protease inhibitors). The cells were lysed by sonication and then centrifuged at 30,000g for 1 h. The soluble fractions of Map or Cdc42 were purified using GST4B resin and further cleaned by anion-exchange column (Source-15Q, Pharmacia) and gel filtration chromatography (Superdex200, Pharmacia) after removal of GST by Precision protease. Map and Cdc42 thus purified were mixed together and subjected again to gel filtration chromatography to obtain a complex in the correct stoichiometry. The Map–Cdc42 complex thus generated was used for crystallization.

Crystallization and data collection

Crystals of the Map–Cdc42 complex were generated by mixing the complex with an equal amount of well solution by the hanging drop vapor diffusion method. The native crystals were crystallized in buffer containing 10% (v/v) PEG 4,000, 0.1 M HEPES, pH 7.0, at room temperature (23–25 °C). The crystals belong to the $P2_12_12_1$ space group, with one complex molecule in each asymmetric unit and a unit cell $a = 41.63 \text{ \AA}$, $b = 83.03 \text{ \AA}$, $c = 99.52 \text{ \AA}$ and $\alpha = \beta = \gamma = 90.0^\circ$. Mercury derivative with a similar unit cell ($a = 41.41 \text{ \AA}$, $b = 83.20 \text{ \AA}$, $c = 99.54 \text{ \AA}$ and $\alpha = \beta = \gamma = 90.0^\circ$) was obtained by soaking the native crystal in the crystallization buffer containing 1.0 mM CH_3HgCl for 24 h at room temperature. Crystals

were equilibrated in a cryoprotectant buffer containing reservoir buffer plus 25.0% (v/v) glycerol. The native and SAD data sets were collected at an in-house beam to 2.3 Å and 2.8 Å, respectively, and processed using the software DENZO and SCALEPACK³⁵.

Structure determination and refinement

The structure of Map–Cdc42 complex was determined using single isomorphous replacement and single anomalous scattering (SIRAS) combined with molecular replacement. Cdc42 was initially positioned using the program MolRep included in CCP4 package³⁶. SOLVE³⁷ was used to locate the positions of mercury. The initial phases from SOLVE were further improved by solvent flattening using RESOLVE³⁷. The model of Map was built into the SIRAS electron density using the program O³⁸. The initial model of Map–Cdc42 complex was first subjected to rigid body refinement and then annealing, position and *B*-factor refinement using CNS³⁹ against the native data set. The final refined atomic model Map–Cdc42 complex contains residues 47–198 from Map and residues 2–26 and 32–178 from Cdc42 and 267 water molecules. Ramachandran plot statistics are as follows: most favored (88.7%), additionally allowed (11.0%), generously allowed (0.3%) and disallowed (0%).

Supplementary Material

Refer to Web version on PubMed Central for supplementary material.

Acknowledgments

We would like to specifically thank J. Dixon (University of California, San Diego), M. Rosen and Kim Orth (University of Texas, Southwestern (UTSW)) for helpful discussion in preparation of this manuscript and for providing valuable reagents, and B. Kenny (Institute for Cell and Molecular Biosciences, Medical School, University of Newcastle) for wild-type EPEC2348/69 and EPEC *map* strains. S.E.S. and A.J.W. are supported by Texas ARP (grant 010019-0085-29007 to N.M.A.) and R.C.O is supported by the Welch foundation (grant I-1704 to N.M.A.). This work was supported by the Rita C. and William P. Clements Jr. endowment for scholars program (UTSW Medical Center) and by the Texas ARP grant 010019-0085-29007 to N.M.A., and by the Chinese Ministry of Science and Technology “863” grant no. 2008AA022305 and “973” grant no. 2006CB806704 to J.C.

References

1. Burrige K, Wennerberg K. Rho and Rac take center stage. *Cell*. 2004; 116:167–179. [PubMed: 14744429]
2. Jaffe AB, Hall A. Rho GTPases: biochemistry and biology. *Annu. Rev. Cell Dev. Biol.* 2005; 21:247–269. [PubMed: 16212495]
3. Rossman KL, Sondek J. Larger than Dbp: new structural insights into RhoA activation. *Trends Biochem. Sci.* 2005; 30:163–165. [PubMed: 15817389]
4. Vetter IR, Wittinghofer A. The guanine nucleotide-binding switch in three dimensions. *Science*. 2001; 294:1299–1304. [PubMed: 11701921]
5. Hart MJ, Eva A, Evans T, Aaronson SA, Cerione RA. Catalysis of guanine nucleotide exchange on the CDC42Hs protein by the dbp oncogene product. *Nature*. 1991; 354:311–314. [PubMed: 1956381]
6. Eva A, Aaronson SA. Isolation of a new human oncogene from a diffuse B-cell lymphoma. *Nature*. 1985; 316:273–275. [PubMed: 3875039]
7. Karnoub AE, et al. Molecular basis for Rac1 recognition by guanine nucleotide exchange factors. *Nat. Struct. Biol.* 2001; 8:1037–1041. [PubMed: 11685227]

8. Snyder JT, et al. Structural basis for the selective activation of Rho GTPases by Dbl exchange factors. *Nat. Struct. Biol.* 2002; 9:468–475. [PubMed: 12006984]
9. Nagai H, Kagan JC, Zhu X, Kahn RA, Roy CR. A bacterial guanine nucleotide exchange factor activates ARF on *Legionella phagosomes*. *Science*. 2002; 295:679–682. [PubMed: 11809974]
10. Amor JC, et al. The structure of RalF, an ADP-ribosylation factor guanine nucleotide exchange factor from *Legionella pneumophila*, reveals the presence of a cap over the active site. *J. Biol. Chem.* 2005; 280:1392–1400. [PubMed: 15520000]
11. Hardt WD, Chen LM, Schuebel KE, Bustelo XR, Galan JE. *S. typhimurium* encodes an activator of Rho GTPases that induces membrane ruffling and nuclear responses in host cells. *Cell*. 1998; 93:815–826. [PubMed: 9630225]
12. Buchwald G, et al. Structural basis for the reversible activation of a Rho protein by the bacterial toxin SopE. *EMBO J.* 2002; 21:3286–3295. [PubMed: 12093730]
13. Alto NM, et al. Identification of a bacterial type III effector family with G protein mimicry functions. *Cell*. 2006; 124:133–145. [PubMed: 16413487]
14. Kenny B, et al. Co-ordinate regulation of distinct host cell signalling pathways by multifunctional enteropathogenic *Escherichia coli* effector molecules. *Mol. Microbiol.* 2002; 44:1095–1107. [PubMed: 12046591]
15. Ohya K, Handa Y, Ogawa M, Suzuki M, Sasakawa C. IpgB1 is a novel *Shigella* effector protein involved in bacterial invasion of host cells: its activity to promote membrane ruffling via Rac1 and Cdc42 activation. *J. Biol. Chem.* 2005; 280:24022–24034. [PubMed: 15849186]
16. Ohlson MB, et al. Structure and function of *Salmonella* SifA indicate that its interactions with SKIP, SseJ, and RhoA family GTPases induce endosomal tubulation. *Cell Host Microbe*. 2008; 4:434–446. [PubMed: 18996344]
17. Handa Y, et al. *Shigella* IpgB1 promotes bacterial entry through the ELMO-Dock180 machinery. *Nat. Cell Biol.* 2007; 9:121–128. [PubMed: 17173036]
18. Derewenda U, et al. The crystal structure of RhoA in complex with the DH/PH fragment of PDZRhoGEF, an activator of the Ca²⁺ sensitization pathway in smooth muscle. *Structure*. 2004; 12:1955–1965. [PubMed: 15530360]
19. Rossman KL, et al. A crystallographic view of interactions between Dbs and Cdc42: PH domain-assisted guanine nucleotide exchange. *EMBO J.* 2002; 21:1315–1326. [PubMed: 11889037]
20. Worthylake DK, Rossman KL, Sondek J. Crystal structure of Rac1 in complex with the guanine nucleotide exchange region of Tiam1. *Nature*. 2000; 408:682–688. [PubMed: 11130063]
21. Aghazadeh B, et al. Structure and mutagenesis of the Dbl homology domain. *Nat. Struct. Biol.* 1998; 5:1098–1107. [PubMed: 9846881]
22. Simpson N, et al. The enteropathogenic *Escherichia coli* type III secretion system effector Map binds EBP50/NHERF1: implication for cell signalling and diarrhoea. *Mol. Microbiol.* 2006; 60:349–363. [PubMed: 16573685]
23. Arbeloa A, et al. Subversion of actin dynamics by EspM effectors of attaching and effacing bacterial pathogens. *Cell. Microbiol.* 2008; 10:1429–1441. [PubMed: 18331467]
24. Hachani A, et al. IpgB1 and IpgB2, two homologous effectors secreted via the Mxi-Spa type III secretion apparatus, cooperate to mediate polarized cell invasion and inflammatory potential of *Shigella flexneri*. *Microbes Infect.* 2008; 10:260–268. [PubMed: 18316224]
25. Beuzón CR, et al. *Salmonella* maintains the integrity of its intracellular vacuole through the action of SifA. *EMBO J.* 2000; 19:3235–3249. [PubMed: 10880437]
26. Boucrot E, Henry T, Borg JP, Gorvel JP, Meresse S. The intracellular fate of *Salmonella* depends on the recruitment of kinesin. *Science*. 2005; 308:1174–1178. [PubMed: 15905402]
27. Brumell JH, Tang P, Mills SD, Finlay BB. Characterization of *Salmonella*-induced filaments (Sifs) reveals a delayed interaction between *Salmonella*-containing vacuoles and late endocytic compartments. *Traffic*. 2001; 2:643–653. [PubMed: 11555418]
28. Stein MA, Leung KY, Zwick M, Garcia-del Portillo F, Finlay BB. Identification of a *Salmonella* virulence gene required for formation of filamentous structures containing lysosomal membrane glycoproteins within epithelial cells. *Mol. Microbiol.* 1996; 20:151–164. [PubMed: 8861213]

29. Berger CN, Crepin VF, Jepson MA, Arbeloa A, Frankel G. The mechanisms used by enteropathogenic *Escherichia coli* to control filopodia dynamics. *Cell. Microbiol.* 2009; 11:309–322. [PubMed: 19046338]
30. García-Mata R, Burridge K. Catching a GEF by its tail. *Trends Cell Biol.* 2007; 17:36–43. [PubMed: 17126549]

References

31. Self AJ, Hall A. Purification of recombinant Rho/Rac/G25K from *Escherichia coli*. *Methods Enzymol.* 1995; 256:3–10. [PubMed: 7476445]
32. Zheng Y, Hart MJ, Cerione RA. Guanine nucleotide exchange catalyzed by dbl oncogene product. *Methods Enzymol.* 1995; 256:77–84. [PubMed: 7476457]
33. Kenny B, Jepson M. Targeting of an enteropathogenic *Escherichia coli* (EPEC) effector protein to host mitochondria. *Cell. Microbiol.* 2000; 2:579–590. [PubMed: 11207610]
34. Alto NM, et al. The type III effector EspF coordinates membrane trafficking by the spatiotemporal activation of two eukaryotic signaling pathways. *J. Cell Biol.* 2007; 178:1265–1278. [PubMed: 17893247]
35. Otwinowski Z, Minor W. Processing of X-ray diffraction data collected in oscillation mode. *Methods Enzymol.* 1997; 276:307–326.
36. Collaborative Computational Project, Number 4. The CCP4 suite: programs for protein crystallography. *Acta Crystallogr. E.* 1994; 50:760–763.
37. Terwilliger T. SOLVE and RESOLVE: automated structure solution, density modification and model building. *J. Synchrotron Radiat.* 2004; 11:49–52. [PubMed: 14646132]
38. Jones TA, Zou JY, Cowan SW, Kjeldgaard M. Improved methods for building protein models in electron density maps and the location of errors in these models. *Acta Crystallogr. A.* 1991; 47:110–119. [PubMed: 2025413]
39. Brünger AT, et al. Crystallography & NMR system: a new software suite for macromolecular structure determination. *Acta Crystallogr. D Biol. Crystallogr.* 1998; 54:905–921. [PubMed: 9757107]

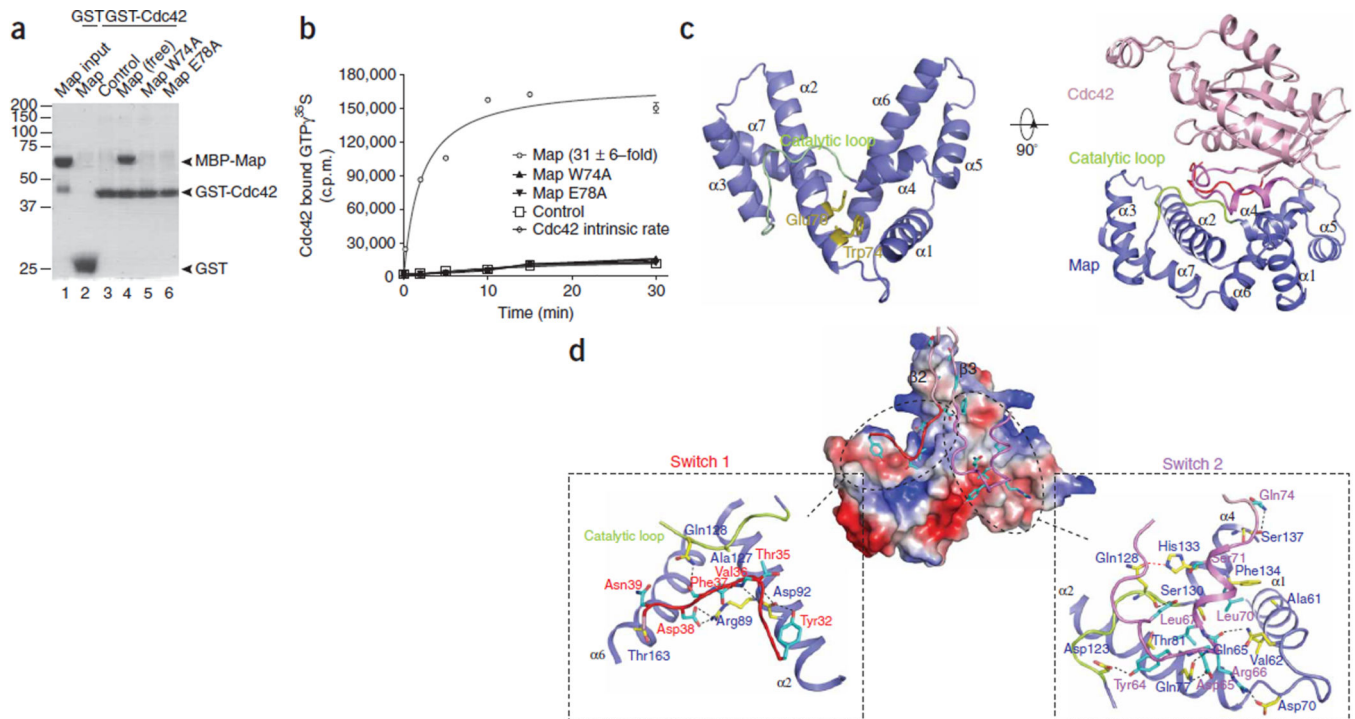
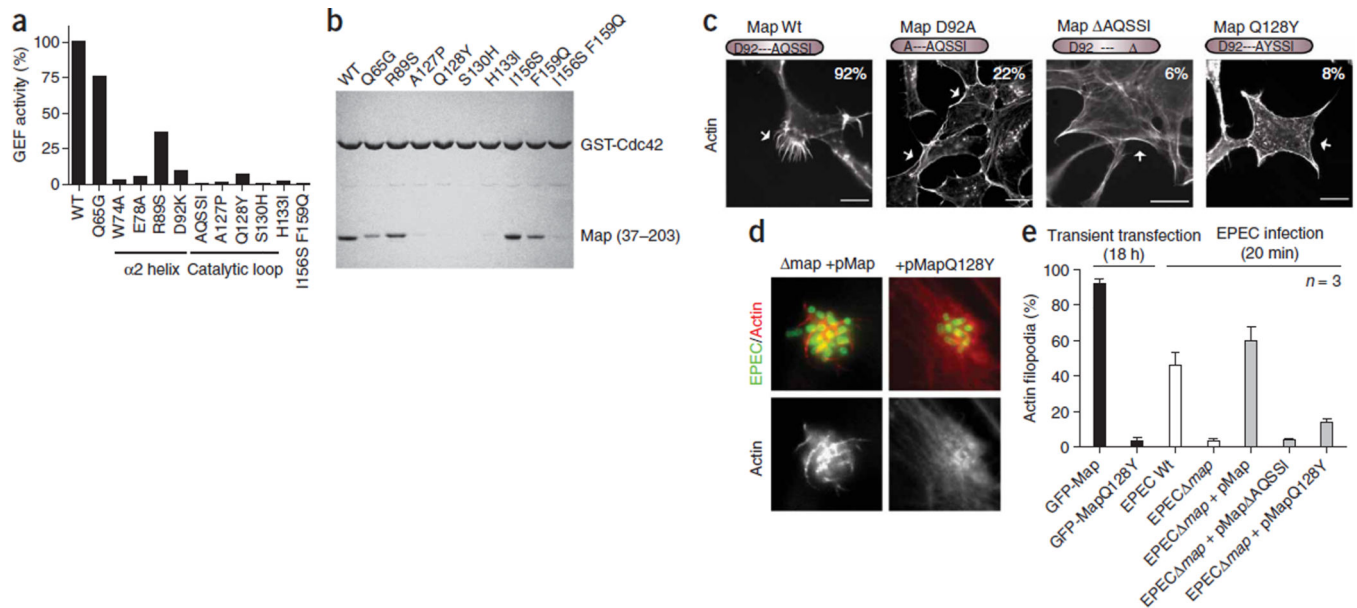


Figure 1.

Biochemical function and structure of Map in complex with Cdc42. **(a)** GST pull-down of 10 μ g GST, or nucleotide-free Cdc42 incubated with 10 μ g MBP (control), MBP-Map residues 37–203, MBP-MapW74A or MBP-Map E78A, as indicated. SDS-PAGE gels stained with Coomassie Brilliant Blue were used to detect protein interactions. Map bound Cdc42 with an apparent 1:1 stoichiometry. In the remainder of experiments, all recombinant Map proteins contained residues 37–203 unless indicated. **(b)** Time course of GTP γ S³⁵ binding assays of 1 μ M Cdc42 and a 0.5 μ M concentration of MBP-Map or the indicated mutant, or intrinsic Cdc42 nucleotide-exchange activity. The average fold activation over intrinsic Cdc42 nucleotide exchange was calculated from the initial slopes of activity from the average of four individual experiments, as reported previously^{7,8}. **(c)** Cartoon representation of the overall structure of Map (left) and Map bound to Cdc42 (right). The α -helices and catalytic loop of Map are labeled. The Trp74 and Glu78 residues of the invariant WxxxE motif are shown in stick representation. **(d)** Overall structure of the Map-Cdc42 complex represented in electrostatic potential surface and ribbon, respectively. Positive and negative charges are in blue and red, respectively. Close-up views of interactions around the switch 1 (red, left) or switch 2 (purple, right) of Cdc42 are shown. The side chains of Map and Cdc42 are shown in yellow and cyan, respectively. Residues involved in interaction are numbered and hydrogen bonds are shown as dashed lines (blue). The intramolecular hydrogen bond is shown in red dashed lines.

**Figure 2.**

Compromise in *in vitro* and *in vivo* activity of Map by mutagenesis. **(a)** Effects of interface mutations in Map on the Cdc42 guanine nucleotide-exchange of $GTP\gamma S^{35}$ catalyzed by 0.5 μM Map (or mutants) as indicated. **(b)** Map (or mutant) protein interactions with Cdc42 as determined by a GST pull-down assay. Wild-type GST-fused Cdc42 was first bound to glutathione Sepharose beads and incubated with Map mutant protein as indicated. After extensive washing, the bound proteins were visualized by Coomassie staining following SDS-PAGE. **(c)** 293A cells transiently transfected with GFP-Map and the indicated mutant constructs were observed by direct fluorescence of rhodamine-phalloidin to detect F-actin. Arrows indicate transfected cells. Only wild-type Map induced cell surface filopodia. **(d)** Pre-activated EPEC *map* strains were incubated with HeLa cells for 20 min and assessed for actin filopodia by rhodamine-phalloidin. The EPEC *map* strain was complemented with a plasmid expressing wild-type Map (pMap) or the catalytic loop mutant MapQ128Y (pMapQ128Y) as indicated. *E. coli* was visualized by Dapi staining. **(e)** Quantification of new actin filopodia in GFP-Map-expressing ($92.3 \pm 3\%$) and GFP-MapQ128Y-expressing ($4.5 \pm 1\%$) cells after 18 h of transfection (left). Quantification of filopodia formation in EPEC infected HeLa cells as indicated. The percentage of EPEC microcolonies with new filopodia after a 20-min infection is indicated. The average of three experiments and s.e.m. are shown.

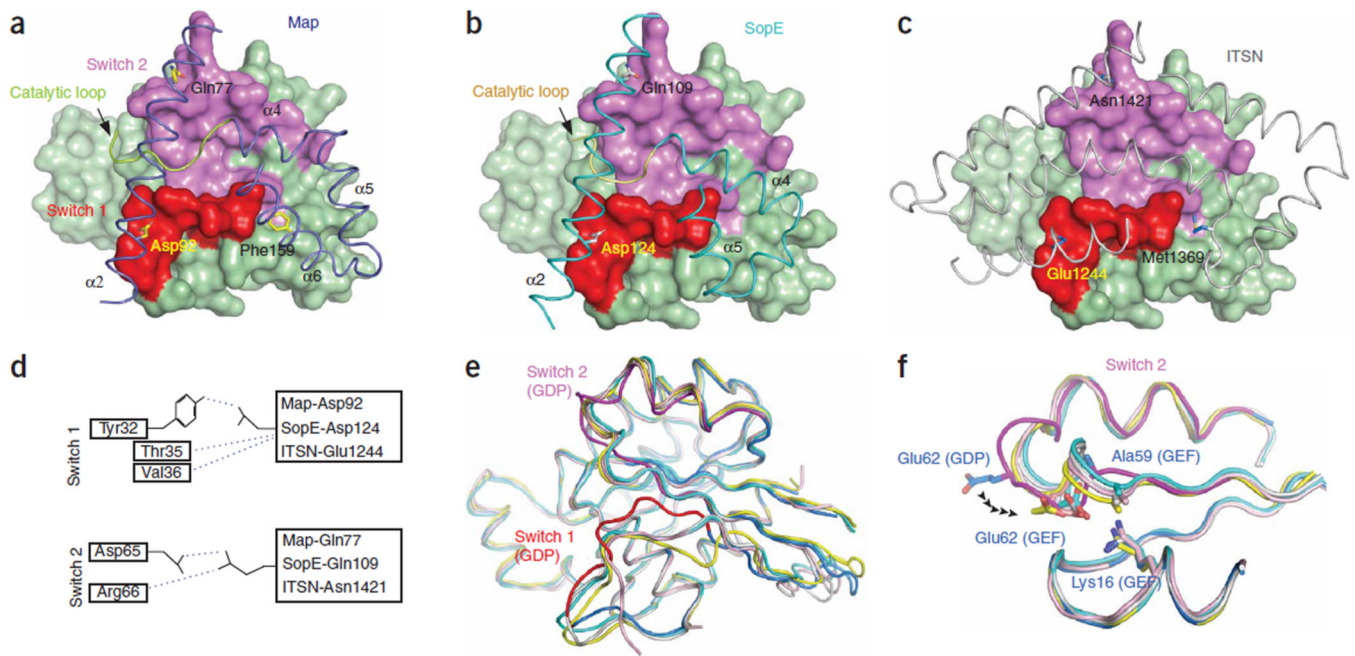
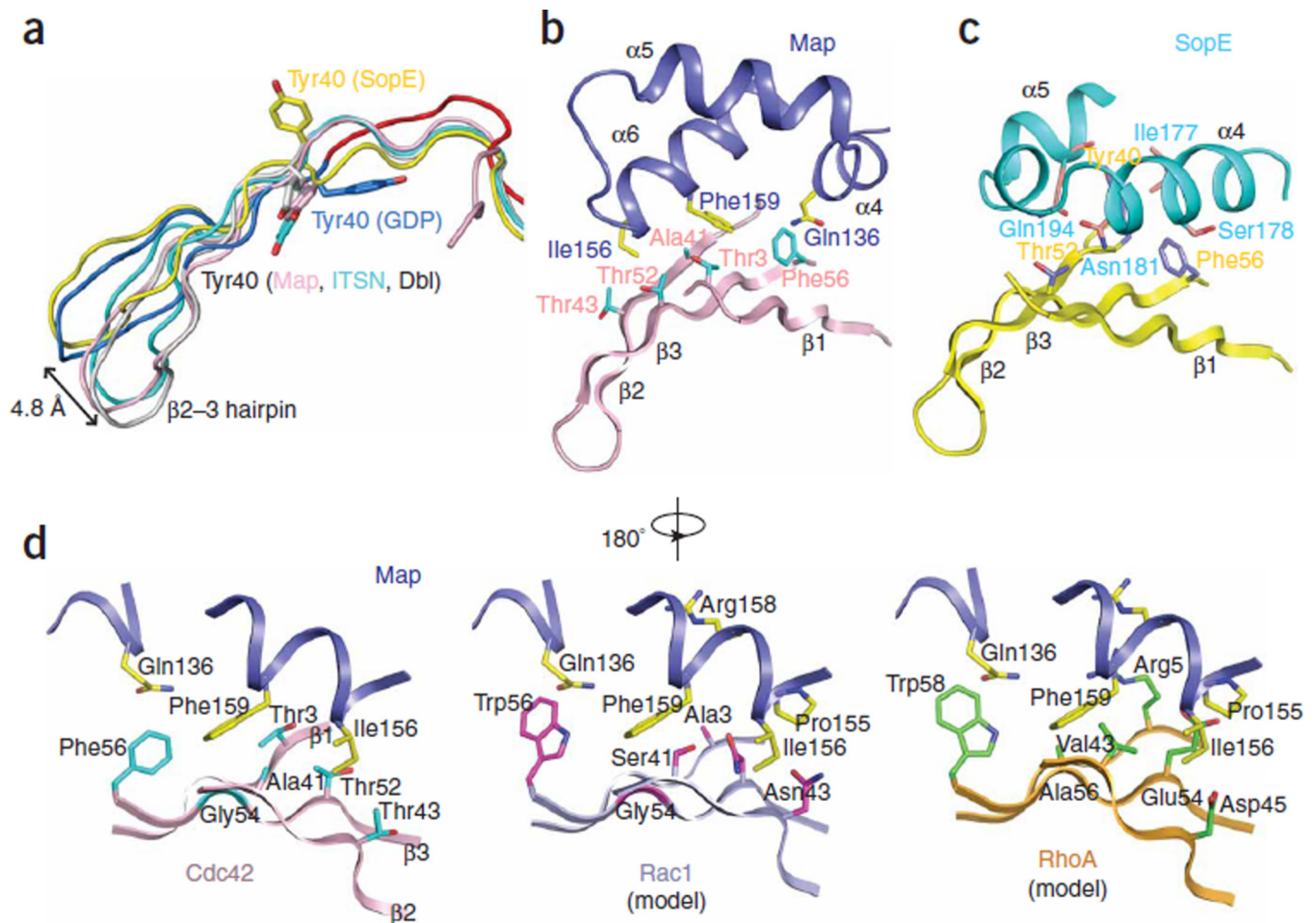
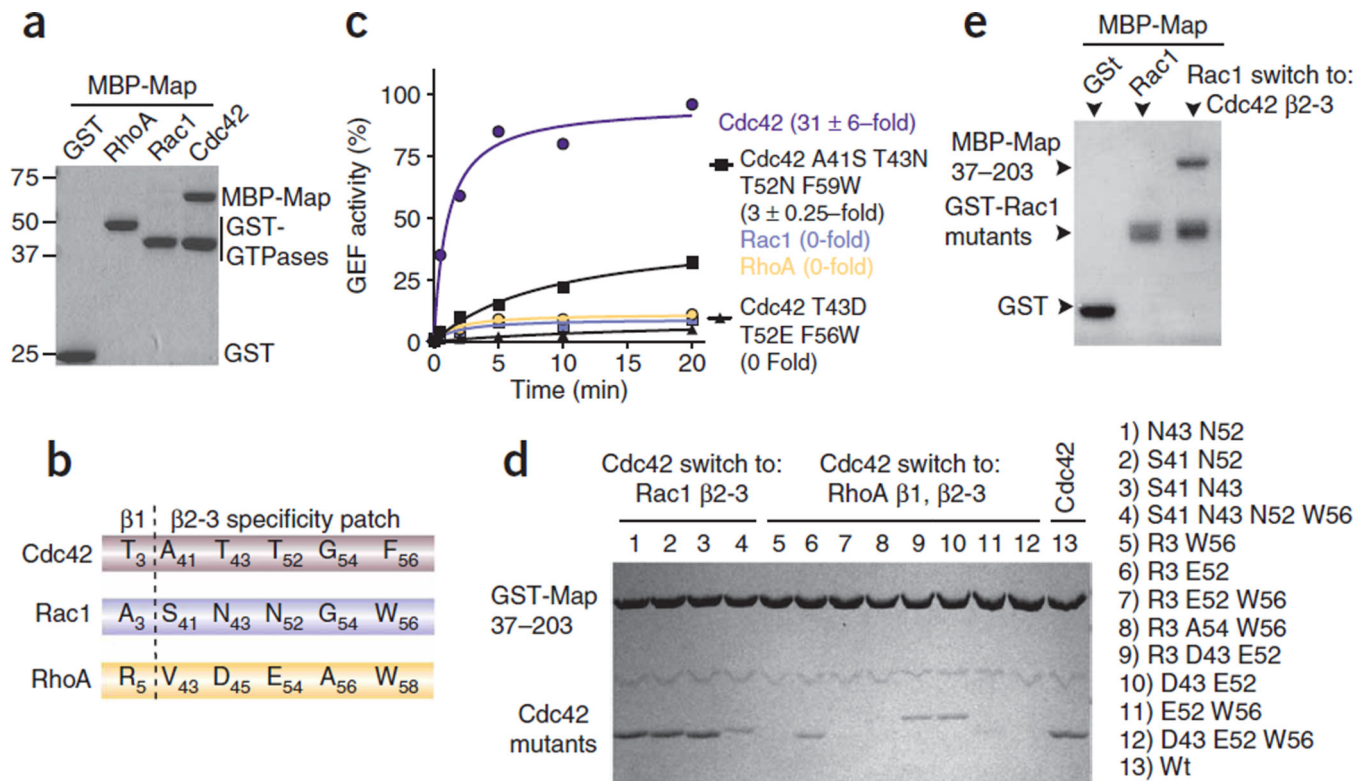


Figure 3. Structural comparison between Map, SopE and ITSN. (a–c) Structure of the Map–Cdc42 complex (a) compared to SopE–Cdc42 (b) and ITSN–Cdc42 (c). Cdc42 is in surface representation and its two switches are colored as indicated. Some secondary-structural elements of Map involved in interaction with Cdc42 are labeled. Cdc42 from the structures of SopE–Cdc42 (PDB 1GZS)¹² and ITSN–Cdc42 (PDB 1KI1)⁸ are shown in the same orientation as in panel a. (d) Hydrogen-bonding residues common between the Map–Cdc42, SopE–Cdc42 and ITSN–Cdc42 structures. Residues and their positions are indicated. (e) Superimposition of Cdc42 and Rac1. Cdc42 from structures of Map–Cdc42 (pink), SopE–Cdc42 (yellow) and ITSN–Cdc42 (gray), and of Rac1 from TIAM1–Rac1 (cyan, PDB 1FOE)²⁰, were used for structural alignment. Important residues and structural elements are assigned based on Cdc42 numbering. ‘GDP’ and ‘GEF’ denote the GDP-bound and GEF-bound forms of the GTPases, respectively. (f) Similar conformational changes around switch 2 are induced by Map and SopE, ITSN and TIAM1. Shown in the figure is the superimposition of Cdc42 and Rac1 around the region of switch 1. The color codes are the same as those in e.

**Figure 4.**

Structural comparison of the Map-Cdc42, SopE-Cdc42 and ISTN-Cdc42 complexes. (a) Close-up view of comparison of GTPase structures around switch 1 and the $\beta 2-3$ hairpin, as described in Figure 3e. The unique positions of Cdc42-Tyr40 and the displacement of the $\beta 2-3$ hairpin in the SopE-Cdc42 structure are indicated. Following binding of Map or ISTN, Cdc42-Gly47 at the tip of $\beta 2-3$ has translated about 4.8 Å and 5.3 Å, respectively, compared to the 2.0 Å shift induced by binding of SopE. (b,c) Structural comparison of Map-Cdc42 and SopE-Cdc42 complexes around $\beta 2-3$ strands of Cdc42. Close-up views of the interaction of $\beta 2-3$ strands of Cdc42 with Map (b) and SopE (c). (d) Structural elements of Map that select against Rac1 and RhoA. A comparison of Map-Cdc42 $\beta 2-3$ structure (left) to two structure-based models obtained by superimposing Rac1 (in Tiam1-Rac1) (middle) and RhoA (in PDZRhoGEF-RhoA) (left panel) onto Map. The backbones of Rac1 and RhoA are in light blue and orange, respectively.

**Figure 5.**

Structural determinants of Cdc42 isoform selection by Map. **(a)** Map selectively binds Cdc42. Glutathione pull-down experiment of GST-tagged RhoA, Rac1 or Cdc42 incubated with equimolar MBP-Map. **(b)** Alignment of the $\beta 1$ and $\beta 2$ -3 Cdc42 interface residues that bind Map compared to the equivalent positions in Rac1 and RhoA. **(c)** Time course of GTP γ S³⁵ nucleotide exchange on Cdc42 (purple), Rac1 (light blue) and RhoA (orange) compared to a mutant Cdc42 whose $\beta 2$ -3 residues are switched to those of Rac1 (A41S T43N T52N F56W, light blue) or to those of Rho (T43D T52E F56W, orange) by 0.5 μ M of Map, as described in Figure 1b. **(d)** Effects of numerous Rac1 and RhoA switch-of-function substitutions in Cdc42 on the binding interaction with Map, as determined by a glutathione pull-down assay. GST-tagged Map residues 37-203 was used to pull down the untagged GTPases and mutants as indicated. **(e)** Glutathione pull-down of GST-tagged Rac1 or mutant Rac1 whose $\beta 2$ -3 residues are switched to those of Cdc42 (S41A N43T N52T W56F) with MBP-tagged Map. Map did not bind Rac1 but bound strongly to the Rac1 mutant.

Table 1

Data collection and refinement statistics for Map–Cdc42 complex

	Native	CH ₃ HgCl
Data collection		
Space group	<i>P</i> ₂ ₁ ₂ ₁	<i>P</i> ₂ ₁ ₂ ₁
Cell dimensions <i>a</i> , <i>b</i> , <i>c</i> (Å)	41.63, 83.03, 99.52	41.41, 83.20, 99.54
Resolution (Å)	2.3 (2.38–2.3)	2.8 (2.85–2.8)
<i>R</i> _{merge}	8.5 (35.8)	11.8 (29.9)
<i>I</i> / σ <i>I</i>	21.5 (5.4)	11.2 (2.6)
Completeness (%)	99.6 (99.9)	93.1 (72.0)
Redundancy	5.2 (5.0)	4.9 (2.4)
Refinement		
Resolution (Å)	20.0–2.3	
No. reflections	15,451	
<i>R</i> _{work} / <i>R</i> _{free}	23.6/27.4	
No. atoms		
Protein	2,582	
Water	249	
<i>B</i> -factors		
Protein	36.2	
Water	39.1	
R.m.s. deviations		
Bond lengths (Å)	0.007	
Bond angles (°)	1.388	

Values in parentheses are for highest-resolution shell.